ACS APPLIED MATERIALS & INTERFACES

Research Article

www.acsami.org

Ionic Charge Transfer Complex Induced Visible Light Harvesting and Photocharge Generation in Perovskite

Tsz-Wai Ng,[†,‡] Hrisheekesh Thachoth Chandran,[†] Chiu-Yee Chan,[†] Ming-Fai Lo,*[,†,‡] and Chun-Sing Lee*[,†,‡]

[†]Center of Super-Diamond and Advanced Films (COSDAF), Department of Physics and Materials Science, City University of Hong Kong, Hong Kong SAR, P. R. China

[‡]City University of Hong Kong Shenzhen Research Institute, Shenzhen 518057, Guangdong, People's Republic of China

Supporting Information

ABSTRACT: Organometal trihalide perovskite has recently emerged as a new class of promising material for high efficiency solar cells applications. While excess ions in perovskites are recently getting a great deal of attention, there is so far no clear understanding on both their formation and relating ions interaction to the photocharge generation in perovskite. Herein, we showed that tremendous ions indeed form during the initial stage of perovskite formation when the organic methylammonium halide (MAX^a, X^a = Br and I) meets the inorganic PbX^b_2 (X^b = Cl, Br, I). The strong charge exchanges between the Pb^{2+} cations and X^{a-} anions result in formation of ionic charge transfer complexes (iCTC). MAX^a parties induce empty valence electronic states within the forbidden bandgap of PbX^b_2. The strong surface dipole provide sufficient driving force for sub-bandgap electron transition with energy identical to the optical bandgap of forming perovskites. Evidences from XPS/UPS and photoluminescence studies showed that the light absorption, exciton dissociation, and photocharge generation of the perovskites are closely related to the strong ionic charge transfer interactions between Pb^{2+} and X^{a-} ions in the perovskite lattices. Our results shed light on mechanisms of light harvesting and subsequent free carrier generation in perovskites.

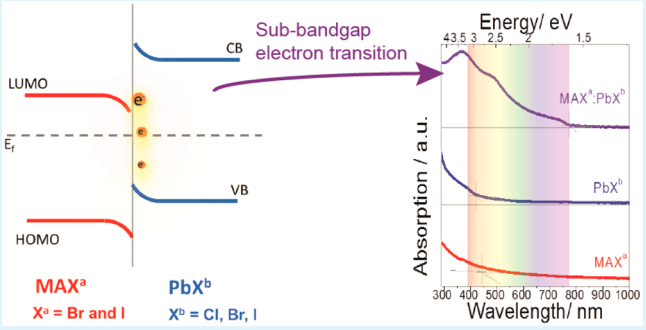

KEYWORDS: *energy level offsets, interface energetics, charge transfer complex, photoemission spectroscopy, perovskite solar cells*

1. INTRODUCTION

Organolead trihalide perovskite is currently one of the most puzzling but interesting materials.[1−7] While perovskite devices have high power conversion efficiencies up to 20.1%,[8] it often exhibits obvious current density−voltage (J-V) hysteresis, which is mainly attributed to interstitial ions in perovskites.[8−12] With these characteristics, perovskite with switchable photovoltaic and memristive effects are observed.[13,14] All these reports point out the obvious role of ionic properties in perovskite.[14] However, there is so far few studies probing the chemical nature of the ions and how these ions pay their role in the photocharge generation.[3,15]

Organometal trihalide perovskites have properties that differ considerably from their constituting components.[16,17] For example, MAI and $PbCl_2$ are themselves wide energy gap semiconductors and therefore are electrically and optically inert. Yet, perovskites show excellent conductivities for both electrons and holes,[1,18−20] as well as broad absorption over the visible spectrum.[19,21−25] Figure S1 (Supporting Information) compares absorption spectra of thin films of MAI, $PbCl_2$, and their mixture (i.e., MAI:$PbCl_2$ with 1:1 weight ratio without heat treatment). While both MAI and $PbCl_2$ themselves show near-UV absorption, their mixture shows significant redshift in absorption, extending to ∼800 nm.[16,17,26,27] It is obvious that the visible absorption in the MAI:$PbCl_2$ mixture is not simply the sum (by ratio) of that of the MAI and $PbCl_2$ constituents.

While increasing attention has been put on the ionic natures of the perovskite film,[26,28,29] fundamental understanding on these ions including their formation, electronic behavior, and their influences to photocharge generation are very limited.[6,16,30,31] The large difference in the absorption spectra of perovskite and its constituents (i.e., MAI and $PbCl_2$) implies a strong charge interaction upon contact between MAI and $PbCl_2$.[17,32−34] However, there are so far few works focusing on the electronic charge interaction between MAI and $PbCl_2$.[3,15] In this work, we explore the ion formation process in the initial perovskite formation upon contact of MAX^a (X^a = Br, I) and PbX^b_2 (X^b = Cl, Br, I) by X-ray and UV photoemission spectroscopies (XPS and UPS). Obvious charge transfers between Pb and X^a are observed in all cases. It is also observed

Received: June 30, 2015
Accepted: August 25, 2015
Published: August 25, 2015

DOI: 10.1021/acsami.5b05847
ACS Appl. Mater. Interfaces 2015, 7, 20280−20284

that the MAX^a would induce empty valence electronic states within the energy gap of PbX^b_2, which facilitates sub-bandgap electron transitions with energies identical to the optical bandgaps of the corresponding perovskites. This result gives a hint on the origin of the band gap and free carrier generation in perovskite.

2. RESULTS AND DISCUSSION

Charge Transfer Properties of the MAI/$PbCl_2$ Film. We first examine charge interaction between MAI and $PbCl_2$. The top spectrum in Figure 1a shows the photoluminescence (PL)

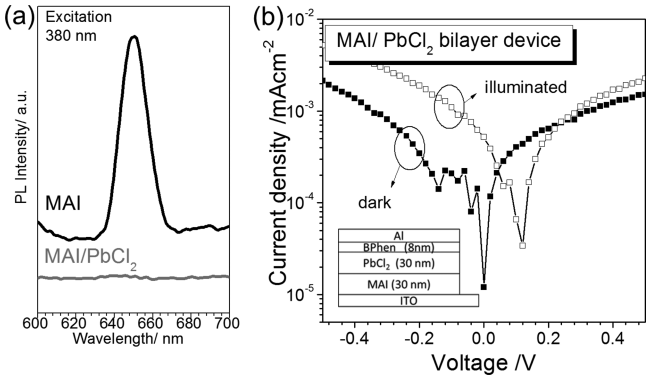

Figure 1. (a) Photoluminescence (PL) response of the MAI film with and without the addlayer $PbCl_2$ quencher film. The testing film is prepared on the Si wafer and excited using 380 nm light. (b) J-V characteristics of the MAI/$PbCl_2$ bilayer device. The solid and open symbols indicate the J-V measured in the dark and under 1 Sun illumination, respectively.

from a pristine MAI film with emission at ~650 nm. When 10 nm $PbCl_2$ was then deposited on top of the MAI film, PL emission of MAI is immediately quenched (bottom spectrum). This result suggests a strong charge exchange crossing the MAI/$PbCl_2$ interface where the photoexcited charges in MAI would be readily dissociated and transferred to its neighboring $PbCl_2$ molecules.

We then probe whether the observed charge transfer properties at MAI/$PbCl_2$ can give photocharge generation. A simple bilayer MAI/$PbCl_2$ device is fabricated with a configuration as follows: ITO/MAI (30 nm)/$PbCl_2$ (30 nm)/BPhen (8 nm)/Al (8 nm). It is noted that the prepared MAI/$PbCl_2$ sample has a neat bilayer structure with no perovskite formation (see Figure S2 (Supporting Information). Figure 1b shows J-V characteristics of the device in the dark and under 1 Sun AM1.5G illumination. The device does show observable photocurrent and photovoltage confirming photocharge generation subsequent to charge dissociation shown in Figure 1a. It is interesting to note that the PL quenching and photovoltaic properties of MAI/$PbCl_2$ are similar to those observed in charge interactive donor−acceptor pairs used in common organic photovoltaics (OPV) devices.[35−38]

Valence Energy Band Structure of Organic−Inorganic Interface. To get a better understanding of the ions in the perovskites, we explore their formation processes by studying charge interaction upon contact between MAX^a and PbX^b_2. 10.0 nm thick MAX^a films were first deposited onto ITO substrates. PbX^b_2 are then incrementally deposited onto the MAX^a samples. UPS of the MAX^a and MAX^a/PbX^b_2 samples were measured. UPS measurements from junctions of MAI/$PbCl_2$, MAI/PbI_2, MABr/PbI_2, and MABr/PbI_2 are shown in Figures S3−S6 (Supporting Information). The UPS results are summarized as three energy level diagrams as shown in Figure 2.

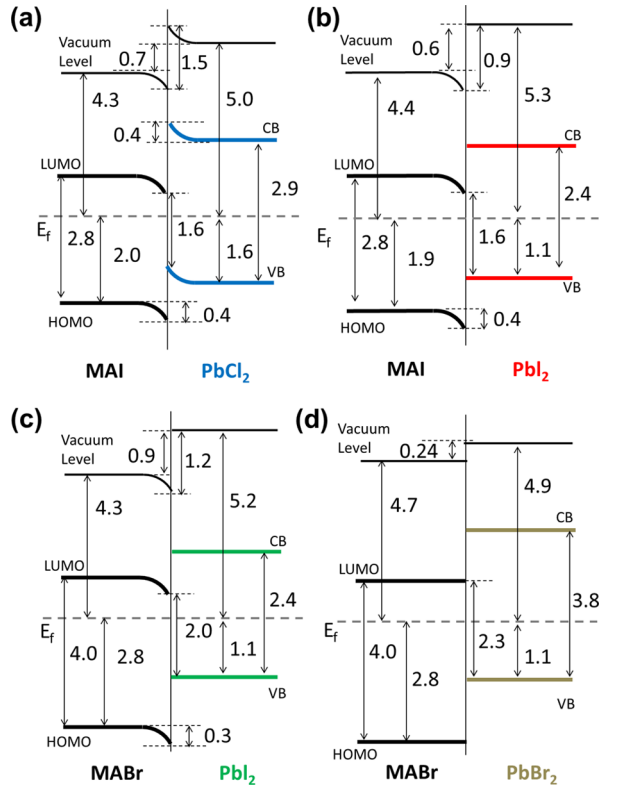

Figure 2. Experimentally determined energy level diagrams of (a) MAI/$PbCl_2$, (b) MAI/PbI_2, (c) MABr/PbI_2, and (d) MABr/$PbBr_2$ junctions. Bandgaps of MAI, MABr, $PbCl_2$, PbI_2, and $PbBr_2$ are determined from the cutoff edges of their optical absorption spectra. All numbers are marked in units of eV.

Abrupt offsets in vacuum levels are observed at the MAI/$PbCl_2$, the MAI/PbI_2, the MABr/PbI_2, and the MABr/$PbBr_2$ contacts with an interfacial dipole of 1.5, 0.9, 1.2, and 0.24 eV, respectively. With such strong dipoles, the MAX^a/PbX^b_2 junction forms a charge-interactive type II heterojunction with strong built-in fields (i.e., similar to the traditional OPV device). Charges exchange are readily taken place between PbX^a_2 and MAX^b. For the junction of MAI/$PbCl_2$, MAI/PbI_2, and MABr/PbI_2, those separated electrons and holes spatially accumulated, resulting in observable energy level bending in the vicinity of the MAX^a and PbX^b_2, respectively. The extent of the charge transfer interaction shows a decreasing order as follows: MAI/$PbCl_2$ > MAI/PbI_2 > MABr/PbI_2 > MABr/$PbBr_2$. One major difference between MAI/$PbCl_2$ and the MAI/PbI_2 junctions is that Cl is unstable in the perovskites lattice.[15,39,40] Most of the Cl has a high tendency to escape from the system and leave the Pb atoms behind. These Pb atoms in the MAI-$PbCl_2$ system are more ready to donate their valence electrons to neighboring MAI, and this leads to a stronger charge transfer compared to MAI/PbI_2 junctions. Therefore, with the strong charge interaction, MAI/$PbCl_2$ shows a charge transfer thickness up to 5−10 nm. For less interactive MABr/PbI_2, MAI/PbI_2, and MABr/$PbBr_2$ junctions, the charge transfer depths are smaller, which are ~2 nm, ~1 nm, and ~0 nm, respectively.

DOI: 10.1021/acsami.5b05847
ACS Appl. Mater. Interfaces 2015, 7, 20280−20284

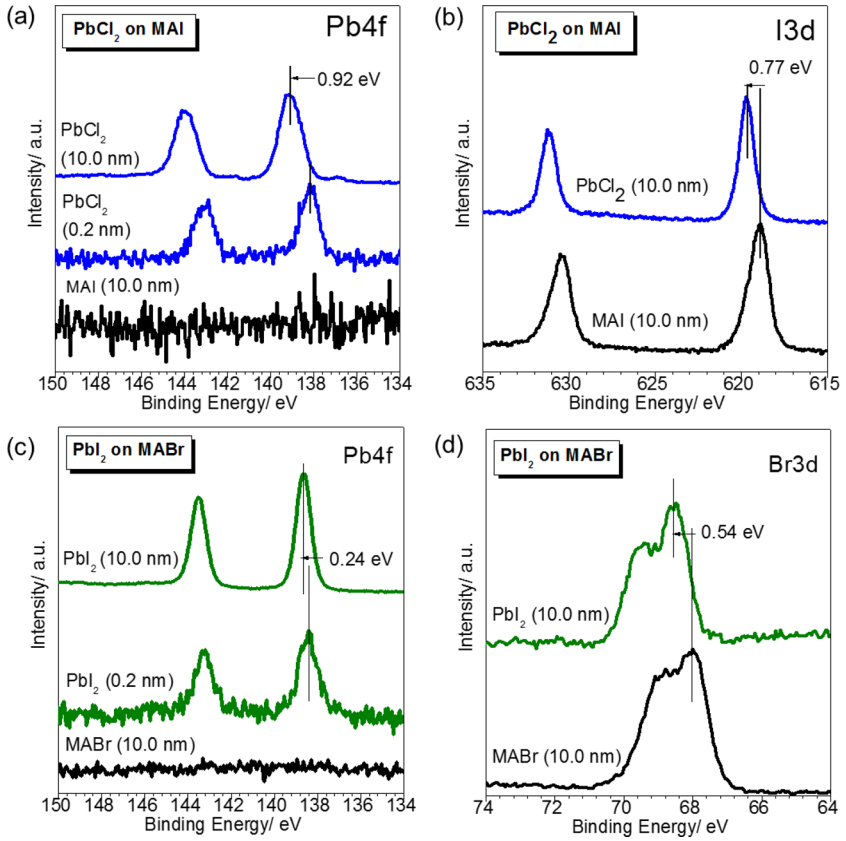

Figure 3. High-resolution XPS core level spectra of (a) Pb 4f and (b) I 3d when different thicknesses of $PbCl_2$ are deposited on 10.0 nm of MAI. XPS core level spectra of (c) Pb 4f and (d) Br 3d when different thicknesses of PbI_2 are deposited on 10.0 nm of MABr.

Interestingly, the VB_{PbX2}—$LUMO_{MAX}$ energy offsets at the MAI/$PbCl_2$, the MAI/PbI_2, the MABr/PbI_2, and the MABr/$PbBr_2$ junction are determined to be 1.6, 1.6, 2.0, and 2.3 eV, respectively, which match well with the optical bandgap of the $MAPbI_{3-x}Cl_x$ (1.6 eV),[30,40,41] MAI/PbI_2 (1.6 eV),[30,40] $MAPbI_{3-x}Br_x$ (1.96 and 2.01 eV for respectively $MAPb(I_{0.41}Br_{0.59})_3$ and $MAPb(I_{0.28}Br_{0.72})_3$),[42] and $MAPbBr_3$ (2.3 eV)[30] perovskites film. The UPS results provide new insight on how the absorption spectrum of perovskite can be extended to the visible region upon mixing of its two wide-bandgap components. The charge interaction between the MAX^a and PbX^b_2 induces a stepping state for sub-bandgap electron transition and photocharge generation. The LUMO of MAX^a behaves as a midgap state within the wide bandgap of PbX^b_2 that provides an empty state for sub-bandgap electron transition. Such electron transition and charge separation provide an interpretation to instant exciton dissociation and photocharge generation within the perovskite lattices.

Apart from excitonic absorption across the bandgap, the electrons can be excited and promoted to the LUMO of MAX^a via visible photon absorption. Such charge interaction is consistent with the PL quenching observed in the MAI/$PbCl_2$ bilayer (Figure 1a), suggesting an intimate charge exchange at the MAI/$PbCl_2$ contact. These observations are consistent with the reported two distinct absorption peaks at ~480 and ~760 nm in common perovskite film.[36,43]

Ionic Charge Transfer Nature of the Organic–Inorganic Contact. Following the discussion on charge transfer interaction at the MAX^a/ PbX^b_2 contact, we examined also the elemental core level XPS peak changes near the MAI/$PbCl_2$ interface. It is interesting to observe that not all elements are contributing to the interfacial charge transfer interaction. Only the Pb^{2+} (Figure 3a) and the I^- (Figure 3b) ions participate in the charge transfer interaction during the MAI/$PbCl_2$ interface formation.[15] Similar XPS peak shifts are observed in Pb^{2+} (Figure 3c) and Br^- (Figure 3d) for the MABr/PbI_2 junction. Meanwhile, the N 1s and C 1s spectra (from $CH_3NH_3^+$, MA^+) shown in Figure S8 (Supporting Information) for both the MAI/$PbCl_2$ and the MABr/PbI_2 junctions show negligible peak shift. The above ionic charge transfer interaction can also be found in heat-treated perovskite film. Similar XPS studies on heat-treated perovskite film are also studied with the data shown in Figure S9 in the Supporting Information. These XPS results suggest that the MA^+ ion has a small active role in the reaction between MAX^a and PbX^b_2. This observation corroborates with the fact that the energy levels of the MA^+ cation are located far away from the valence band maximum VBM (5 eV below) and conduction band minimum CBM (2.5 eV above) of the perovskite film.[44,45]

Together with these XPS results, we confirm that the valence charge exchange observed in UPS (Figure 2) is mainly attributed to ionic interaction between X^{a-} and Pb^{2+} ions in MAX^a/PbX^b_2. The initial contact of X^{a-} and Pb^{2+} ions has strong charge interactions, which finally result in formation of the ionic charge transfer complex (iCTC) with special long wavelength absorption characteristics. Depending on the extent of charge transfer, these iCTC are free to rotate and migrate toward two electrodes when they are subjected to E-field from either external applied bias or illumination, leading to bistable conductance (hysteresis effect).

DOI: 10.1021/acsami.5b05847
ACS Appl. Mater. Interfaces 2015, 7, 20280–20284

3. CONCLUSION

In this work, we show for the first time the photocharge generation process in perovskite film is closely related to the ionic charge exchange process at the contacts of MAX^a and PbX^b_2. Direct evidence from both XPS and UPS showed that the ionic charge exchange process that has taken place between the Pb^{2+} cation and the X^{a-} anion is strong enough to induce an ionic charge transfer complex formation. In addition, such interaction leads to a sub-bandgap electron transition via the LUMO level of MAX^a which is located within the wide energy gap of PbX^b_2. The energy band offsets are found to match well with the optical bandgaps of the corresponding perovskites. The presented results shed light on light harvesting and free carrier generation of the perovskite-based cells.

4. EXPERIMENTAL SECTION

Device Fabrication. Solar devices were prepared on patterned and routinely cleaned indium-doped tin oxide (ITO) coated glasses. The ITO substrate is UV-ozone treated for 15 min prior to loading into an evaporation system with a base pressure of $\sim 10^{-7}$ Torr. All evaporating sources including MAI, C_{60}, BPhen (from Luminescence Technology Corp.), and $PbCl_2$ (form Aldrich) are used as received. A simple device with a configuration of ITO/MAI (30 nm)/$PbCl_2$ (30 nm)/BPhen (8 nm)/Al is prepared by thermal evaporation. No intentional annealing was included during and after device fabrication. The freshly prepared device is then transferred to a nitrogen-filled glovebox, where it is encapsulated with a glass cap and UV curing epoxy resin. J-V characteristics of the device are characterized using an Oriel 150 W solar simulator with AM1.5G (AM: air mass, G: global) filters at 100 mW/cm^2. More details can be found in our previous report.[46]

All photoemission studies are carried out in a VG ESCALAB 220i-XL surface analysis system equipped with a He-discharge lamp ($h\nu$ = 21.22 eV) and a monochromatic Al−Kα X-ray gun ($h\nu$ = 1486.6 eV) for UPS and XPS investigation, respectively. The base vacuum of the system is 10^{-9} Torr. ITO-coated glass substrates were thoroughly cleaned before loading into the ultrahigh vacuum (UHV). 10.0 nm of MAX^a (X^a = I and Br) is first deposited onto the ITO substrate. The PbX^b_2 (X^b = Cl, I, and Br) layer of 0.2−10.0 nm thick is then deposited onto the MAX^a samples. Between each deposition, the samples are transferred to the analysis chamber without vacuum break for UPS and XPS characterizations. UPS He I measurements are performed to study the valence states of the prepared films. VL offsets are obtained from the shifts of the intensity thresholds at the lowest inelastic electrons kinetic energy cutoff, with a bias of −5.0 V with respect to ground. Energy gaps of the MAX^a and PbX^b_2 are estimated by considering cutoff edges of their absorption spectra as shown in the Supporting Information.

■ ASSOCIATED CONTENT

Supporting Information

The Supporting Information is available free of charge on the ACS Publications website at DOI: 10.1021/acsami.5b05847.

Figures S1−S9 (PDF)

■ AUTHOR INFORMATION

Corresponding Authors

*E-mail: mingflo@cityu.edu.hk (M.-F.L.).
*E-mail: apcslee@cityu.edu.hk (C.-S.L.).

Notes

The authors declare no competing financial interest.

■ ACKNOWLEDGMENTS

This work was supported by a grant from the Research Grants Council of the Hong Kong Special Administrative Region, China (Project No. T23-713/11) and the National Natural Science Foundation of China (No. 21303150 and No. 51473138).

■ REFERENCES

(1) Burschka, J.; Pellet, N.; Moon, S. J.; Humphry-Baker, R.; Gao, P.; Nazeeruddin, M. K.; Gratzel, M. Sequential Deposition as a Route to High-performance Perovskite-sensitized Solar Cells. *Nature* **2013**, *499* (7458), 316−319.

(2) Chen, Q.; Zhou, H. P.; Hong, Z. R.; Luo, S.; Duan, H. S.; Wang, H. H.; Liu, Y. S.; Li, G.; Yang, Y. Planar Heterojunction Perovskite Solar Cells via Vapor-Assisted Solution Process. *J. Am. Chem. Soc.* **2014**, *136* (2), 622−625.

(3) Lo, M. F.; Guan, Z. Q.; Ng, T. W.; Chan, C. Y.; Lee, C. S. Electronic Structures and Photoconversion Mechanism in Perovskite/Fullerene Heterojunctions. *Adv. Funct. Mater.* **2015**, *25* (8), 1213−1218.

(4) Marchioro, A.; Teuscher, J.; Friedrich, D.; Kunst, M.; van de Krol, R.; Moehl, T.; Gratzel, M.; Moser, J. E. Unravelling the Mechanism of Photoinduced Charge Transfer Processes in Lead Iodide Perovskite Solar Cells. *Nat. Photonics* **2014**, *8* (3), 250−255.

(5) Gonzalez-Pedro, V.; Juarez-Perez, E. J.; Arsyad, W. S.; Barea, E. M.; Fabregat-Santiago, F.; Mora-Sero, I.; Bisquert, J. General Working Principles of CH3NH3PbX3 Perovskite Solar Cells. *Nano Lett.* **2014**, *14* (2), 888−893.

(6) Kim, H. S.; Mora-Sero, I.; Gonzalez-Pedro, V.; Fabregat-Santiago, F.; Juarez-Perez, E. J.; Park, N. G.; Bisquert, J. Mechanism of Carrier Accumulation in Perovskite Thin-absorber Solar Cells. *Nat. Commun.* **2013**, *4*, 2242.

(7) Edri, E.; Kirmayer, S.; Mukhopadhyay, S.; Gartsman, K.; Hodes, G.; Cahen, D. Elucidating the Charge Carrier Separation and Working Mechanism of CH3NH3PbI3-xClx Perovskite Solar Cells. *Nat. Commun.* **2014**, *5*, 3461.

(8) Jeon, N. J.; Noh, J. H.; Yang, W. S.; Kim, Y. C.; Ryu, S.; Seo, J.; Seok, S. I. Compositional Engineering of Perovskite Materials for High-Performance Solar Cells. *Nature* **2015**, *517* (7535), 476−480.

(9) Zhou, H.; Chen, Q.; Li, G.; Luo, S.; Song, T.-b.; Duan, H.-S.; Hong, Z.; You, J.; Liu, Y.; Yang, Y. Interface Engineering of Highly Efficient Perovskite Solar Cells. *Science* **2014**, *345* (6196), 542−546.

(10) McGehee, M. D. Perovskite Solar Cells: Continuing to Soar. *Nat. Mater.* **2014**, *13* (9), 845−846.

(11) Mei, A.; Li, X.; Liu, L.; Ku, Z.; Liu, T.; Rong, Y.; Xu, M.; Hu, M.; Chen, J.; Yang, Y. A Hole-Conductor−Free, Fully Printable Mesoscopic Perovskite Solar Cell with High Stability. *Science* **2014**, *345* (6194), 295−298.

(12) Snaith, H. J.; Abate, A.; Ball, J. M.; Eperon, G. E.; Leijtens, T.; Noel, N. K.; Stranks, S. D.; Wang, J. T.-W.; Wojciechowski, K.; Zhang, W. Anomalous Hysteresis in Perovskite Solar Cells. *J. Phys. Chem. Lett.* **2014**, *5* (9), 1511−1515.

(13) Xiao, Z.; Yuan, Y.; Shao, Y.; Wang, Q.; Dong, Q.; Bi, C.; Sharma, P.; Gruverman, A.; Huang, J. Giant Switchable Photovoltaic Effect in Organometal Trihalide Perovskite Devices. *Nat. Mater.* **2015**, *14* (2), 193−198.

(14) Park, N.-G. Perovskite Solar Cells: Switchable Photovoltaics. *Nat. Mater.* **2015**, *14*, 140−141.

(15) Ng, T. W.; Chan, C. Y.; Lo, M. F.; Guan, Z. Q.; Lee, C. S. Formation Chemistry of Perovskites with Mixed Iodide/Chloride Content and the Implications on Charge Transport Properties. *J. Mater. Chem. A* **2015**, *3*, 9081−9085.

(16) Wang, Q. K.; Wang, R. B.; Shen, P. F.; Li, C.; Li, Y. Q.; Liu, L. J.; Duhm, S.; Tang, J. X. Energy Level Offsets at Lead Halide Perovskite/Organic Hybrid Interfaces and Their Impacts on Charge Separation. *Adv. Mater. Interfaces* **2015**, *2* (3), 1400528−1400534.

(17) Ng, T. W.; Lo, M. F.; Fung, M. K.; Zhang, W. J.; Lee, C. S. Charge-Transfer Complexes and Their Role in Exciplex Emission and Near-Infrared Photovoltaics. *Adv. Mater.* **2014**, *26* (31), 5569−5574.

DOI: 10.1021/acsami.5b05847
ACS Appl. Mater. Interfaces 2015, 7, 20280−20284

(18) Im, J. H.; Lee, C. R.; Lee, J. W.; Park, S. W.; Park, N. G. 6.5% Efficient Perovskite Quantum-dot-sensitized Solar Cell. *Nanoscale* **2011**, *3* (10), 4088−4093.
(19) Yin, W. J.; Shi, T. T.; Yan, Y. F. Unusual Defect Physics in CH3NH3PbI3 Perovskite Solar cell Absorber. *Appl. Phys. Lett.* **2014**, *104* (6), 063903.
(20) You, J.; Hong, Z.; Yang, Y. M.; Chen, Q.; Cai, M.; Song, T.-B.; Chen, C.-C.; Lu, S.; Liu, Y.; Zhou, H. Low-Temperature Solution-Processed Perovskite Solar Cells with High Efficiency and Flexibility. *ACS Nano* **2014**, *8*, 1674−1680.
(21) Mitzi, D. B. Solution-Processed Inorganic Semiconductors. *J. Mater. Chem.* **2004**, *14* (15), 2355−2365.
(22) Bi, D. Q.; Yang, L.; Boschloo, G.; Hagfeldt, A.; Johansson, E. M. J. Effect of Different Hole Transport Materials on Recombination in CH3NH3PbI3 Perovskite-Sensitized Mesoscopic Solar Cells. *J. Phys. Chem. Lett.* **2013**, *4* (9), 1532−1536.
(23) Wang, Y.; Gould, T.; Dobson, J. F.; Zhang, H. M.; Yang, H. G.; Yao, X. D.; Zhao, H. J. Density Functional Theory Analysis of Structural and Electronic Properties of Orthorhombic Perovskite CH3NH3PbI3. *Phys. Chem. Chem. Phys.* **2014**, *16* (4), 1424−1429.
(24) Mitzi, D. B.; Chondroudis, K.; Kagan, C. R. Organic-Inorganic Electronics. *IBM J. Res. Dev.* **2001**, *45* (1), 29−45.
(25) Kim, H.-S.; Lee, C.-R.; Im, J.-H.; Lee, K.-B.; Moehl, T.; Marchioro, A.; Moon, S.-J.; Humphry-Baker, R.; Yum, J.-H.; Moser, J. E.; Grätzel, M.; Park, N.-G. Lead Iodide Perovskite Sensitized All-Solid-State Submicron Thin Film Mesoscopic Solar Cell with Efficiency Exceeding 9%. *Sci. Rep.* **2012**, *2*, 591−597.
(26) Jeng, J. Y.; Chen, K. C.; Chiang, T. Y.; Lin, P. Y.; Tsai, T. D.; Chang, Y. C.; Guo, T. F.; Chen, P.; Wen, T. C.; Hsu, Y. J. Nickel Oxide Electrode Interlayer in CH3NH3PbI3 Perovskite/PCBM Planar-Heterojunction Hybrid Solar Cells. *Adv. Mater.* **2014**, *26* (24), 4107−4113.
(27) Yan, K.; Wei, Z.; Li, J.; Chen, H.; Yi, Y.; Zheng, X.; Long, X.; Wang, Z.; Wang, J.; Xu, J. High-Performance Graphene-Based Hole Conductor-Free Perovskite Solar Cells: Schottky Junction Enhanced Hole Extraction and Electron Blocking. *Small* **2015**, *11* (19), 2269−2274.
(28) Jeng, J. Y.; Chiang, Y. F.; Lee, M. H.; Peng, S. R.; Guo, T. F.; Chen, P.; Wen, T. C. CH3NH3PbI3 Perovskite/Fullerene Planar-Heterojunction Hybrid Solar Cells. *Adv. Mater.* **2013**, *25* (27), 3727−3732.
(29) Zhu, Z.; Ma, J.; Wang, Z.; Mu, C.; Fan, Z.; Du, L.; Bai, Y.; Fan, L.; Yan, H.; Phillips, D. L. Efficiency Enhancement of Perovskite Solar Cells Through Fast Electron Extraction: The Role of Graphene Quantum Dots. *J. Am. Chem. Soc.* **2014**, *136* (10), 3760−3763.
(30) Schulz, P.; Edri, E.; Kirmayer, S.; Hodes, G.; Cahen, D.; Kahn, A. Interface Energetics in Organo-metal Halide Perovskite-based Photovoltaic Cells. *Energy Environ. Sci.* **2014**, *7* (4), 1377−1381.
(31) Liu, P.; Liu, X.; Lyu, L.; Xie, H.; Zhang, H.; Niu, D.; Huang, H.; Bi, C.; Xiao, Z.; Huang, J. Interfacial Electronic Structure at the CH3NH3PbI3/MoOx Interface. *Appl. Phys. Lett.* **2015**, *106* (19), 193903.
(32) Zhang, T.; Zhao, B.; Chu, B.; Li, W.; Su, Z.; Yan, X.; Liu, C.; Wu, H.; Gao, Y.; Jin, F.; Hou, F. Simple Structured Hybrid WOLEDs Based on Incomplete Energy Transfer Mechanism: From Blue Exciplex to Orange Dopant. *Sci. Rep.* **2015**, *5*, 10234.
(33) Ng, T. W.; Lo, M. F.; Lee, S. T.; Lee, C. S. Exciplex Emission and its Relationship with Depletion Organic Heterojunction. *Org. Electron.* **2012**, *13* (9), 1641−1645.
(34) Park, Y. S.; Lee, S.; Kim, K. H.; Kim, S. Y.; Lee, J. H.; Kim, J. J. Exciplex-Forming Co-host for Organic Light-Emitting Diodes with Ultimate Efficiency. *Adv. Funct. Mater.* **2013**, *23*, 4914−4920.
(35) Veldman, D.; Meskers, S. C. J.; Janssen, R. A. J. The Energy of Charge-Transfer States in Electron Donor-Acceptor Blends: Insight into the Energy Losses in Organic Solar Cells. *Adv. Funct. Mater.* **2009**, *19* (12), 1939−1948.
(36) Xing, G. C.; Mathews, N.; Sun, S. Y.; Lim, S. S.; Lam, Y. M.; Gratzel, M.; Mhaisalkar, S.; Sum, T. C. Long-Range Balanced Electron- and Hole-Transport Lengths in Organic-Inorganic CH3NH3PbI3. *Science* **2013**, *342* (6156), 344−347.
(37) Stranks, S. D.; Eperon, G. E.; Grancini, G.; Menelaou, C.; Alcocer, M. J. P.; Leijtens, T.; Herz, L. M.; Petrozza, A.; Snaith, H. J. Electron-Hole Diffusion Lengths Exceeding 1 Micrometer in an Organometal Trihalide Perovskite Absorber. *Science* **2013**, *342* (6156), 341−344.
(38) McNeill, C. R.; Halls, J. J. M.; Wilson, R.; Whiting, G. L.; Berkebile, S.; Ramsey, M. G.; Friend, R. H.; Greenham, N. C. Efficient Polythiophene/Polyfluorene Copolymer Bulk Heterojunction Photovoltaic Devices: Device Physics and Annealing Effects. *Adv. Funct. Mater.* **2008**, *18* (16), 2309−2321.
(39) Yu, H.; Wang, F.; Xie, F.; Li, W.; Chen, J.; Zhao, N. The Role of Chlorine in the Formation Process of "CH3NH3PbI3-xClx" Perovskite. *Adv. Funct. Mater.* **2014**, *24* (45), 7102−7108.
(40) Colella, S.; Mosconi, E.; Fedeli, P.; Listorti, A.; Gazza, F.; Orlandi, F.; Ferro, P.; Besagni, T.; Rizzo, A.; Calestani, G. MAPbI3-xCl x Mixed Halide Perovskite for Hybrid Solar Cells: The Role of Chloride as Dopant on the Transport and Structural Properties. *Chem. Mater.* **2013**, *25* (22), 4613−4618.
(41) Luo, S.; Daoud, W. A. Recent Progress in Organic−Inorganic Halide Perovskite Solar Cells: Mechanisms and Material Design. *J. Mater. Chem. A* **2015**, *3* (17), 8992−9010.
(42) Kulkarni, S. A.; Baikie, T.; Boix, P. P.; Yantara, N.; Mathews, N.; Mhaisalkar, S. Band-gap Tuning of Lead Halide Perovskites using a Sequential Deposition Process. *J. Mater. Chem. A* **2014**, *2* (24), 9221−9225.
(43) Manser, J. S.; Kamat, P. V. Band Filling With Free Charge Carriers in Organometal Halide Perovskites. *Nat. Photonics* **2014**, *8* (9), 737−743.
(44) Brivio, F.; Walker, A. B.; Walsh, A. Structural and Electronic Properties of Hybrid Perovskites for High-Efficiency Thin-Film Photovoltaics from First-Principles. *APL Mater.* **2013**, *1* (4), 042111.
(45) Giorgi, G.; Fujisawa, J. I.; Segawa, H.; Yamashita, K. Cation Role in Structural and Electronic Properties of 3D Organic-Inorganic Halide Perovskites: A DFT Analysis. *J. Phys. Chem. C* **2014**, *118* (23), 12176−12183.
(46) Lo, M. F.; Ng, T. W.; Mo, H. W.; Lee, C. S. Direct Threat of a UV-Ozone Treated Indium-Tin-Oxide Substrate to the Stabilities of Common Organic Semiconductors. *Adv. Funct. Mater.* **2013**, *23* (13), 1718−1723.

DOI: 10.1021/acsami.5b05847
ACS Appl. Mater. Interfaces 2015, 7, 20280−20284